THE JOURNAL OF PHYSICAL CHEMISTRY C

Article

Cite This: J. Phys. Chem. C 2018, 122, 28884−28894

pubs.acs.org/JPCC

# Diffusivity, Interfacial Free Energy, and Crystal Nucleation in a Supercooled Lennard-Jones Liquid

Azat O. Tipeev,*[,†] Edgar D. Zanotto,[‡] and José P. Rino[†]

[†]Department of Physics, Federal University of São Carlos, Via Washington Luiz, km. 235, 13.565-905 São Carlos, SP, Brazil

[‡]Department of Materials Engineering, Federal University of São Carlos, Via Washington Luiz, km. 235, 13.565-905 São Carlos, SP, Brazil

**ABSTRACT:** We carried out extensive molecular dynamics simulations of seeded crystallization in a Lennard-Jones liquid in a wide range of supercoolings under zero external pressure. The number of particles in the critical crystal nucleus, $n_*$, the particle transport coefficient at the liquid/nucleus interface, $\mathcal{D}_*$, the crystal pressure, $p_{s*}$, the crystal density, $\rho_{s*}$, and the thermodynamic driving force, $\Delta\mu = p_{s*}/\rho_{s*}$, were determined at 11 temperatures. We used the classical nucleation theory (CNT) to calculate the effective nucleus/liquid interfacial free energy, $\gamma_e$. The results of seeded crystallization fit rather well to those of a previous work on spontaneous crystallization and show that $\gamma_e$ monotonically increases with temperature. Using the physical properties determined from the computer simulations: $p_{s*}$, $\rho_{s*}$, $n_*$, $\mathcal{D}_*$, $\Delta\mu$, and the equilibrium melting temperature, we calculated the steady-state crystal nucleation rates, $J(T)$. The agreement with a value determined from spontaneous nucleation was excellent, demonstrating the validity of the CNT, as opposed to the often-reported colossal discrepancies between the theoretical and experimental values of nucleation rates. A key factor to explain this agreement is that we used correct, directly determined physical parameters. In this work, $n_*(T)$, $\Delta\mu(T)$, and $\mathcal{D}_*(T)$ obtained from the simulations were used instead of (fitted) average interfacial energy, calculated $\Delta\mu$, and other approximations, such as viscosity or nucleation timelags, for the transport term in the analysis of experimental nucleation rates.

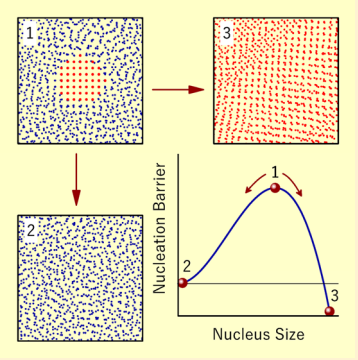


## I. INTRODUCTION

Supercooled liquids retain the properties of their parent liquid phase after being cooled below the equilibrium melting point. This metastable (against the isochemical crystalline phase) state starts to decay with the appearance of heterophase fluctuations that eventually lead to the birth of a critical nucleus of the stable crystalline phase. This metastable state corresponds to a local free energy minimum, and the transition to a stable state caused by crystal nucleation is associated with the overcoming of an energy barrier,[1] which depends on the material's composition, mechanism, and conditions of the process.

The kinetics of spontaneous homogeneous crystal nucleation in supercooled liquids has frequently been described (semiquantitatively) by the classical nucleation theory, CNT.[2] In accordance with this theory, for a spherical nucleus, the height of the nucleation barrier (i.e., the work of formation of a critical nucleus, $W_*$) is given by

$$W_* = \frac{16\pi}{3} \times \frac{\gamma_e^3}{\rho_{s_*}^2 \times \Delta\mu^2} \tag{1}$$

where $\rho_{s*}$ is the number density of the critical crystal nucleus (i.e., the inverse of the molecular volume), $\Delta\mu$ is the difference between the chemical potentials of the crystal phase and the supercooled liquid, which is negative, and $\gamma_e$ is the effective value of the critical nucleus/supercooled liquid interfacial free energy.[3]

This required work for nucleation corresponds to a critical nucleus of radius

$$R_* = \frac{2\gamma_e}{\rho_{s_*} \times |\Delta\mu|} \tag{2}$$

In the case of isobaric supercooling, $\Delta\mu$ can be approximated by the following expression,[4] which gives an upper bound:

$$\Delta\mu = \frac{\Delta h_m \Delta T}{T_m} \tag{3}$$

where $\Delta T = T_m - T$, $T_m$ is the equilibrium temperature, and $\Delta h_m$ is the melting enthalpy. Other expressions can be used for $\Delta\mu$, for instance:[5−7]

$$\Delta\mu = \frac{\Delta h_m \Delta T}{T_m} \frac{T}{T_m} \tag{4}$$

$$\Delta\mu = \frac{\Delta h_m \Delta T}{T_m} \frac{2T}{T_m + T} \tag{5}$$

Received: October 31, 2018
Revised: November 21, 2018
Published: November 26, 2018






DOI: 10.1021/acs.jpcc.8b10637
J. Phys. Chem. C 2018, 122, 28884−28894

$$\Delta\mu = \frac{\Delta h_m \Delta T}{T_m}\frac{7T}{T_m + 6T} \quad (6)$$

Later on, we will compare the calculations using these expressions with the value of $\Delta\mu$ obtained from the computer simulations.

If an embryo exceeds a critical size, $R > R_*$ (eq 2), it becomes a supercritical nucleus that can spontaneously grow, leading to a phase transition. In a system under constant temperature and pressure, after a certain time-lag (which is strongly dependent on the liquid composition and temperature), a stationary nucleation rate, $J$, can be established. In this case, the number of viable nuclei formed per unit of time per unit volume is given by[8]

$$J = \rho \mathcal{D}_* Z_* \exp(-W_*/k_B T) \quad (7)$$

where $\rho$ ($m^{-3}$) is the number of particles per unit volume, $\mathcal{D}_*[s^{-1}]$ is the effective coefficient of transport across the liquid/nucleus interface, which is determined by the mechanism of particle aggregation to the nucleus, $k_B$ is the Boltzmann constant, and $Z_*$ is the dimensionless Zeldovich factor, which characterizes the curvature of the energy barrier in the critical region and takes into account the dissolution of a fraction of supercritical nuclei

$$Z_* = \left(\frac{W_*/k_B T}{3\pi n_*^2}\right)^{1/2} \quad (8)$$

where $n_*$ is the number of particles in the critical nucleus. For most cases of interest, $Z_* = 0.01-0.10$.[2]

Expression 7 is the main equation of the classical theory of nucleation. Accordingly, the steady-state nucleation rate, $J(T)$, depends essentially on $\mathcal{D}_*$, which typically has an exponential (or stronger) temperature dependence, and $W_*/k_B T$ (the so-called thermodynamic barrier or Gibbs number). CNT is theoretically valid if the thermodynamic barrier is higher than $k_B T$, $W_* > k_B T$.

Finally, using eqs 1, 2, 8, we can write eq 7 as

$$J = \rho \mathcal{D}_* \left(\frac{|\Delta\mu|}{6\pi n_* k_B T}\right)^{1/2} \exp\left(-\frac{n_*|\Delta\mu|}{2k_B T}\right) \quad (9)$$

Turnbull and Fisher[9] obtained the following expression for evaluating the kinetic coefficient at (approximately) the saddle point of the potential barrier

$$\mathcal{D}_* = i_*(k_B T/h) \exp(-E/k_B T) \quad (10)$$

where $i_*$ is the number of atoms on the surface of a critical nucleus, $h$ is the Planck constant, and $E$ is the activation energy for the transition of atoms from the supercooled liquid into the crystalline nuclei, which can vary with temperature, $E = E(T)$. In describing crystallization processes in real materials, $E$ is normally not known and is usually approximated by the activation energy of atomic or molecular self-diffusion, or of viscous flow in the supercooled liquid.[10]

Experiments on homogeneous crystallization using various methods clearly indicate the possibility of formation of a crystalline phase in supercooled liquids.[3,11] Experimental investigation of homogeneous nucleation is possible by eliminating heterogeneous centers, by purifying or fragmenting the sample,[12] which leads to the predominant contribution of homogeneously dispersed nuclei to overall crystallization, which sometimes appear in supercooled liquids.[3] However, experimental studies of the early stage of phase transition are rather complicated due to the nanometric size and insignificant volume fraction of the critical nuclei. In most cases, such as in nucleation of glass-forming systems, indirect methods are used to develop the nuclei at high temperatures to detectable sizes and then follow their nucleation kinetics.[13,14]

Only some scarce examples of direct measurements of crystal nucleation have been performed. For example, apoferritin crystallization was observed at the microscopic level using atomic force microscopy.[15] Due to the large size of the molecules and their low crystallization rate, the appearance of new crystals could be traced as a function of time and temperature. The authors found that nuclei containing $n = 20-50$ molecules continuously form and disintegrate, where as larger fluctuations of supercritical size grow. Similar behavior was observed in the crystallization of certain concentrated colloidal suspensions.[16,17]

Nevertheless, experimental studies of spontaneous nucleation in supercooled liquids are difficult. First, according to the expression 1, the quantity $W_*$ strongly depends on the interfacial free energy, $\gamma_e$, of the boundary between the critical nucleus and the maternal phase. At present, there are no reliable methods for the experimental measurement of $\gamma_e$. Therefore, in crystallization studies, $\gamma_e$ is normally considered a "free", adjustable parameter in eq 1 and, consequently, also in eq 7. This problem precludes the direct comparison of experimental nucleation rates with theoretical calculations. Second, real experiments, determining the nucleation rate as a function of supercooling, are not able to directly measure some important characteristics of the process, such as the size of the critical nucleus. Furthermore, in most cases, the effective transport coefficient at the nucleus/liquid interface, $\mathcal{D}_*$, is not known, hence researchers employ the additional assumption that $\mathcal{D}_*$ is inversely related to the liquid viscosity.[10] Finally, it is very challenging to investigate experimentally crystallization processes with very low or very high nucleation rates; only $10^4 < J$, $s^{-1}$ $m^{-3} < 10^{18}$ can be experimentally probed.[10]

Fortunately, however, new possibilities of learning about this essential microscopic process are available by powerful computer simulation methods: molecular dynamics (MD) and Monte Carlo. The MD method allows the study of crystallization at a microscopic level, in a region of states that are not yet attainable in laboratory experiments, to obtain information on the properties of the (nanosized) crystalline nuclei, and to test nucleation theories.[11] The most widely used and simplest, in terms of the computational implementation technique, is the "mean lifetime" method.[3] In accordance with this technique, the nucleation rate is assumed to be in steady-state and is calculated by $J = 1/\bar{\tau}V$, where $\bar{\tau}$ is the average waiting time for the appearance of the first viable nucleus of the new phase and $V$ is the volume of the simulation box. However, the mean lifetime method (a brute-force numerical technique) has limitations regarding the system size and the simulation time, which depend on the speed of the supercomputers used. Since homogeneous nucleation is a random, stochastic process, in which the probability of spontaneous formation of a viable nucleus is directly proportional to the volume of the metastable phase, for brute-force MD nucleation studies, the investigated system needs to be deeply supercooled, typically to $T < 0.8T_m$. Homogeneous crystallization can then be examined only in a range of extremely high nucleation rates, $J \approx 10^{30}-10^{35}$ $s^{-1}$ $m^{-3}$,[11] which correspond to relatively small Gibbs numbers:



DOI: 10.1021/acs.jpcc.8b10637
J. Phys. Chem. C 2018, 122, 28884−28894

$W_*/k_BT \approx 11-22$.[18,19] The study of homogeneous nucleation by the mean lifetime method in thermodynamic states with a higher energy barrier would require a very significant improvement in computational resources.

In recent years, two other approaches have been developed that study the nucleation process at moderate and low supercooling degrees in computer experiments.[11] (i) Enhanced-sampling methods, such as umbrella sampling,[20] metadynamics,[21] transition interface sampling,[22] forward flux sampling[23] and transition path sampling.[24] (ii) The seeding method, in which a crystalline cluster of variable size is inserted into a supercooled liquid at the beginning of the simulation.[11] If the cluster is larger than the critical size at the study temperature, it will tend to grow, whereas subcritical nuclei (embryos) dissolve in the liquid. This clever approach allows the direct determination of the critical size, $n_*$, as a function of temperature. Then, using the CNT formalism, the temperature dependences can be calculated of the effective interfacial free energy of the critical crystal nuclei/liquid and the work of their formation. In this case, the obtained value of $\gamma_e$ is averaged over the crystallographic orientations, and the error is lower than the error when $\gamma_e$ is calculated by the capillary fluctuation method.[25] Most importantly, in this case $n_*$ can be obtained directly from the simulations and used in eq 9 to test the CNT.

The errors of the seeding method are determined by the technique chosen for seed insertion and choice of the seed's thermodynamic and structural properties. Typically, the crystal seed parameters are chosen to correspond those of the bulk crystalline stable phase at any given temperature. However, if the actual nuclei have different properties (e.g., different structure) then the seeding procedure will not reflect the real physical situation. We will show later in this article that, in our case, the nucleation parameters resulting from the used seeding procedure agreed quite well to those ensuing from spontaneous nucleation. It should be noted that the crystal seeding method has also been widely used experimentally in optimizing and controlling engineering crystallization processes in the preparation of crystalline substances with predetermined properties.[26,27]

In MD simulations, the seeding method was first used in 2000 to crystallize germanium[28] at one temperature. The authors found in that study at $T = 0.625T_m$ that the spherical critical nucleus radius is $R_* = 1$ nm. The seeding technique was also used to unveil the crystallization of atomic and molecular model systems. For instance: Si,[29−31] colloidal fluid,[32,33] Lennard-Jones (LJ),[34−41] $Cu_{50}Zr_{50}$,[42,43] Ni,[42−44] Cr,[44] $H_2O$,[36,45−56] hard spheres,[36,57−61] $Ge_2Sb_2Te_5$,[62] methane hydrate,[63] Cu,[25,64] Fe,[65,66] Au,[67] NaCl,[36,68−70] Potts lattice model,[71] 2D LJ,[72] and Al.[73] The number of particles in the embedded embryos ranged from $n = 13$[37−40] to 39000,[36] and the Gibbs number reached the upper value of $W_*/k_BT \approx 1100$.[36]

In most of the above listed papers[25,28−73] on the crystal seeding method, including the frequently cited ref 35, no comparison was made of the obtained nucleation rate, $J$, with its direct calculation at the same temperature for the same model system. Only in five of them[36,47,50,68,70] the authors extrapolated the $J(T)$ calculated by the seeding method at moderate supercoolings to $J$ data obtained by a brute-force method at high supercoolings. The discrepancy ranged from 1 to 6 orders of magnitude. It should be observed that these differences seem to be large, but they are much smaller than the often reported discrepancies of 20−55 o.m. in experimental studies.[10]

Only in ref 36, for model systems of $H_2O$, NaCl, and hard spheres, there have been comparisons of the interfacial free energy, $\gamma_e$, obtained by the seeding method with the values of $\gamma_e$ calculated by the CNT for data resulting from umbrella sampling. Finally, to the best of our knowledge, only in refs 47 and 61 have there been a comparison of the number of atoms in the critical nuclei $n_*$ obtained by the seeding method, with independent determinations by the mean first passage time (MFPT) method[74] and the forward flux sampling, showing their self-consistency. In this article, we also make such comparisons for $\gamma_e$ and $n_*$.

Turning to LJ liquids, the object of this study, Bai and Li[34,35] and Espinosa et al.[36] used the seeding method to study the crystallization of a supercooled liquid at zero pressure. They established[34−36] that $\gamma_e(T)$ is a linearly increasing function of temperature, but the reported values of $\gamma_e$ at the studied temperatures were different.

By linearly extrapolating the values of $\gamma_e(T)$ up to the temperature of equilibrium melting, the free energy of the flat (macroscopic) interface between the crystal and liquid phases, $\gamma_\infty$, can be estimated. In refs 35 and 36, this approach led to values of $\gamma_\infty$, differing by 19%. Finally, recently[18] values of $\gamma_e$ were calculated by using the CNT from homogeneous nucleation rate data in the region of deep supercoolings, where spontaneous nucleation was detected and studied by brute-force MD simulations. The obtained values $\gamma_e(T)$ differ by up to 10% from the calculations of $\gamma_e$ by the seeding method of ref 35.

Therefore, the main objectives of this study are (i) to obtain, by atomistic simulation, a full picture of the nucleus/liquid interfacial free energy (the most important parameter of CNT) in a wide range of temperatures, and (ii) to test the validity of the CNT in predicting crystal nucleation rates in a supercooled liquid.

To accomplish this task, we studied the crystallization of a one-component LJ liquid on a zero isobar via MD simulations by the seeding technique. The values of $\gamma_e$ at 11 temperatures were calculated using eq 2 with the values of $n_*$, $\Delta\mu$, and $\rho_{s*}$ obtained from the simulations. We also compared the direct determined (spontaneous) nucleation rates of ref 18 with CNT calculations using physical parameters derived from the current MD simulations of seeded crystallization. In section II, we present the MD model under investigation and the computing procedure. The results and discussions are given in section III. Section IV presents the summary and conclusions.

## II. MD MODEL AND THE SEEDING METHOD

**MD Model.** Most experimental studies of crystallization of supercooled liquids are carried out at constant (atmospheric) pressure. Therefore, in this work, we also investigate crystallization at a constant pressure ($p = 0$) to reveal the temperature dependence of nucleation parameters. Molecular dynamics simulations were carried out in an NpT ensemble, ensuring the constancy of the number of particles $N$, pressure $p$, and the temperature $T$ of the system. The particles were located in a cubic cell with 3D periodic boundary conditions. The interparticle interaction was given by the Lennard-Jones pair potential modified by Broughton and Gilmer:[75]


DOI: 10.1021/acs.jpcc.8b10637
J. Phys. Chem. C 2018, 122, 28884−28894

$$\phi(r) = \begin{cases} 4\varepsilon\left[\left(\frac{\sigma}{r}\right)^{12} - \left(\frac{\sigma}{r}\right)^{6}\right] + c_1, & r \le 2.3\sigma \\ c_2\left(\frac{\sigma}{r}\right)^{12} + c_3\left(\frac{\sigma}{r}\right)^{6} + c_4\left(\frac{r}{\sigma}\right)^{2} + c_5, & 2.3\sigma < r < 2.5\sigma \\ 0, & 2.5\sigma \le r \end{cases} \tag{11}$$

where $c_1 = 0.016132\varepsilon$, $c_2 = 3136.6\varepsilon$, $c_3 = -68.069\varepsilon$, $c_4 = -0.083312\varepsilon$, and $c_5 = 0.74689\varepsilon$. The interaction potential 11 is constructed so that at the cutoff radius $r_c = 2.5\sigma$ both the energy and force become zero, whereas the classical LJ interaction potential has a first-order discontinuity at $r = r_c$. The potential parameters $\sigma = 0.3405$ nm and $\varepsilon = 119.8k_B$ K, the particle mass, $m = 6.63 \times 10^{-26}$ kg, and the Boltzmann constant, $k_B$, were used to reduce the calculated quantities, which are denoted by the superscript *, viz. density $\rho^* = \rho\sigma^3$, potential energy $E^*_{pot} = E_{pot}/\varepsilon$, temperature $T^* = k_BT/\varepsilon$, pressure $p^* = p\sigma^3/\varepsilon$, time $t^* = t/\sqrt{m\sigma^2/\varepsilon}$, interfacial free energy $\gamma^* = \gamma\sigma^2/\varepsilon$, nucleation rate $J^* = J\sigma^4\sqrt{m/\varepsilon}$, and interfacial transport coefficient $\mathcal{D}^*_* = \mathcal{D}_*\sigma/\sqrt{\varepsilon/m}$.

MD calculations were carried out in the LAMMPS program.[76] The time step of integrating the equations of particle motion was $\Delta t^* = 0.00231832$, which corresponds to 5 fs. Updating the list of neighboring particles was done within a radius of 0.1 nm every 50 fs.

For the substance with the potential given by eq 11, the parameters of the triple point were determined by different methods[18,75,77−83] and equations of state of the liquid and solid phases in the stable and metastable regions were constructed.[72,82,84,85] In ref 18, the parameters of the melting line were obtained from the condition of real ($\mu = \mu_s$) and mechanical ($p = p_s$) equilibrium. At $p \approx 0$, they found that $T^*_m = 0.618$, $\rho^*_{m_L} = 0.8288$, $\rho^*_{m_S} = 0.9456$, and $\Delta h_m = 1.0339$. In this article, we studied the crystallization kinetics of a supercooled LJ liquid in the supercooled temperature range $T^* = 0.452-0.5535$, corresponding to $T = (0.731-0.896)T_m$.

The interfacial free energy at the crystal/liquid equilibrium coexistence, $\gamma_\infty$, was calculated directly.[75,77,78,86−89] The value of $\gamma_\infty$ obtained by different methods: cleaving potential,[75] cleaving wall,[77] capillary fluctuation,[78] thermodynamic integration,[86,89] mold integration,[87] and metadynamics[88] were in good agreement. The anisotropy of $\gamma_\infty$ was clearly revealed; at the triple point, the crystallographic orientations (100), (110), and (111) averaged value is $\gamma_\infty = 0.360(2)$;[77] the number in brackets indicates the uncertainty in the last significant digit.

**Seeding Method.** The seeding method consists of artificially embedding small crystalline clusters of different sizes (shapes, structures, etc.) of a stable phase into a metastable substance, and in determining the thermodynamic state ($p$, $T$) at which the nucleus becomes critical, that is, the probability of growth and dissolution are equal.

A good quantitative indicator of the evolution of a liquid−crystal seed system is given by its enthalpy[35] or potential energy, $E_{pot}$.[45,67] A sharp decrease of $E_{pot}$ indicates growth of the inserted nucleus and the beginning of a phase transition. In the case of dissolution of the nucleus, the value of $E_{pot}$ remains approximately unaltered.

In accordance with expression 2, for a critical nucleus containing $n_*$ particles, we have

$$n_* = \frac{32\pi}{3} \times \frac{\gamma_e^3}{\rho_{s_*}^2 |\Delta\mu|^3} \tag{12}$$

While the value of $\rho s_*$ can be obtained directly from an MD experiment, the MD method does not lead to a direct determination of the chemical potential, $\Delta\mu$. However, this parameter can be estimated by eqs 3−6 or by eq 13, defined below, which relies on two properties that are obtained from MD.

To check the validity of the CNT, we calculated $\Delta\mu$ (at $p = 0$) as

$$\Delta\mu = \frac{p_{s_*}}{\rho_{s_*}} \tag{13}$$

The pressure in the critical crystal nucleus, $p_{s*}$, can be obtained from the condition of equality of the chemical potentials of a supercooled liquid and a critical nucleus $\mu(p,T) = \mu_{s*}(p_{s*},T)$. With the use of the equation of state of the LJ substance, it is possible to determine the value of $\rho_{s*}$ for any given $p_{s*}$ and $T$.

Therefore, the value of $\gamma_e$ at each temperature was calculated from eq 12, and then the work of the critical nucleus formation results from eq 1, and finally the nucleation rate can be estimated by eq 9. For this last operation, the effective atomic transport coefficient at the liquid/nucleus interface, $\mathcal{D}_*$ (from MD simulations) must also be known.

As noted in earlier works,[36,47] the seeding technique may incorrectly estimate the number of atoms in the nucleus due to its numerous surface atoms, especially for very small-sized clusters. Therefore, it is necessary to combine this method with some independent approach for estimating the critical size, for example, the MFPT.[74] Another weakness of the seeding approach is the a priori acceptance of the validity of CNT for the calculation of $\gamma_e$. Hence, a reliable independent method of direct calculation of the interfacial free energy of the critical nuclei is also needed which, to the best of our knowledge, has not yet been developed.

**Seeding Parameters.** The metastable (supercooled) liquid used here contained $N = 3 \times 10^4$ LJ particles and was obtained by isobaric cooling from a stable state with a rate of $\Delta T^*/\Delta t^* = 10^{-4}$ ($\approx 5.6 \times 10^9$ K/s) and equilibrating during 0.5 ns. At the geometrical center of the supercooled liquid, spheres of radius (0.72−2.18) nm were selected. Then, the liquid particles inside the spheres were removed, and the space was filled with a fragment of a perfect fcc crystal.

We have determined 11 temperatures at which the embedded crystal nucleus of different sizes became critical. Each simulation run only had a single seed in the supercooled liquid. The number of particles in the inserted clusters varied from $n = 43$ to 1055. Fifty independent configurations of supercooled liquids containing a cluster of the same size were studied for reliable statistics. The interaction of the crystal particles was described by the same LJ potential, eq 11 (note that the seeding method can be also used to study two-component crystallization, by changing the interaction potential of the embedding crystal and maternal phase[41,53,54]). The temperature of the crystal nucleus was set to be equal to the temperature of the metastable liquid; and its density was equalized to the density of a stable (bulk) crystal phase at which the liquid and crystal chemical potentials are the same at the given temperature $\mu_{s*}(p_{s*},T) = \mu(p,T)$.[18]



DOI: 10.1021/acs.jpcc.8b10637
J. Phys. Chem. C 2018, 122, 28884−28894

To prevent atomic overlapping, after inserting the seed during 0.05 ns, the maximum displacement of the liquid particles was limited in magnitude by 3.4 pm, and the forces acting on the crystal particles were zeroed. We have found that by using the sixth order Steinhardt parameter q6[90,91] to identify the crystal-like particles, during this period the crystal seeds grew by 30−50%. After equilibrating, during 0.5 ns, the potential energy of the whole system, $E_{pot}$, was calculated every 5 ps, and the coordinates of all particles were recorded.

To test the influence of box size on the kinetics of seeded crystallization, liquid systems containing $N = 3 \times 10^3$ and $3 \times 10^5$ particles were also prepared.

## III. RESULTS AND DISCUSSION

Figure 1 shows two typical time dependences of the potential energy of a supercooled liquid with an inserted crystallite seed,

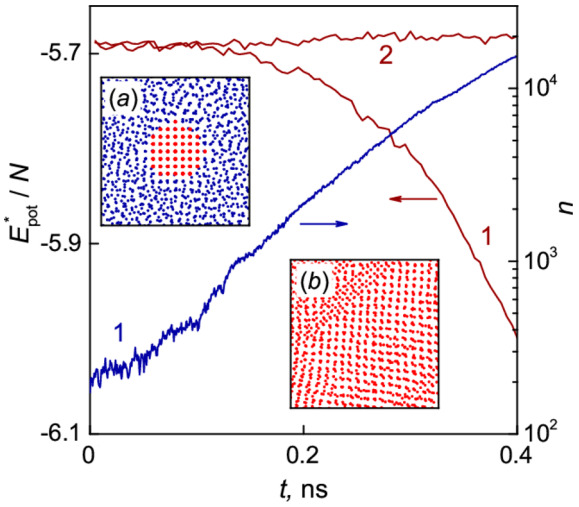


**Figure 1.** Time dependence of the potential energy of the liquid/crystal seed system, $E_{pot}$, and the number of particles, $n$, in the crystal seed, $T = 0.809T_m$: 1, seed growth; 2, seed decay. The values of $E_{pot}$ are normalized by the total number of particles in a two-phase system. Two 2D projections (a $16\sigma \times 16\sigma$ layer of $5\sigma$ thick) of the system configuration are also shown: (a) supercooled liquid containing an inserted crystal seed and (b) crystallized liquid.

$E_{pot}(t)$. A slight increase of $E_{pot}$ (less than 1%, the curve 2 in Figure 1) indicates the dissolution of the crystalline seed, whereas a decrease (the curve 1) is related to the ordering of the atoms of the liquid phase due to crystallization. In the last case, after full crystallization, the value of $E_{pot}$ is still larger than for the ideal crystalline ordering at any given temperature. This is due to the presence of defects in the lattice of the crystalline solid formed by the seed growth. Figure 1 also shows the time dependence of the number of particles in the crystal seed, $n(t)$. Crystal-like particles were identified by the q6 parameter.[90,91] The dependencies $E_{pot}(t)$ and $n(t)$ correlate rather well.

In favorable conditions, critical nuclei could be formed in a metastable liquid containing an embedded seed.[37,40] However, in this study, during the observation of the seed evolution in the metastable liquid ($\Delta t' = 0.5$ ns), spontaneous formation of supercritical sized nuclei did not occur. In ref 18, at $T = 0.728T_m$, the homogeneous nucleation rate was $J^* = 1.6(1) \times 10^{-8}$. Hence, the mean waiting time for the critical nucleus $\tau = 1/(J \times V)$ in the system used ($N = 3 \times 10^4$ particles confined in the volume $V \approx 1.3 \times 10^3$ nm$^3$) is about 5 ns, which is an order of magnitude longer than the interval $\Delta t'$ used. That is why we did not observe the precipitation of new nuclei in the current research.

With regard to the $E_{pot}(t)$ data, the temperatures at which seeds of different sizes became critical were determined. Figure 2 shows the temperature dependence of the number of

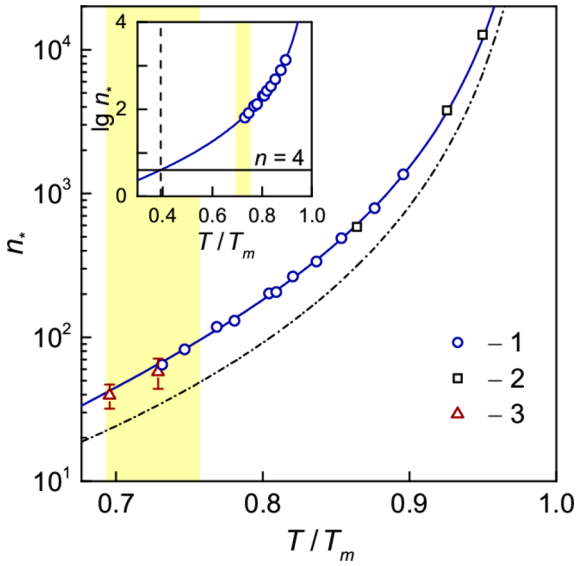


**Figure 2.** Number of particles in the critical crystal nucleus, $n_*$, as a function of supercooling, $T/T_m$, at $p = 0$: 1, current calculations by the seeding method; 2, data of Espinosa et al.;[36] 3, calculations by the MFPT method.[18] The solid line is the CNT fitting. The dash-dotted line shows the data of Bai and Li.[35] Inset: extrapolation of $n_*(T)$ to the deeper supercoolings. The temperature range of spontaneous homogeneous crystallization from a study by a brute-force MD[18] is shown in yellow.

particles in the critical crystal seed, $n_*$. The quantity $n_*$ decreases monotonically with decreasing temperature, as predicted by the CNT. The error in the determination of the temperature does not exceed 1%, which is comparable with the average thermal fluctuations in the liquid in the current $NpT$ ensemble. The radii of the critical nuclei were estimated by $R_* = (3n_*/4\pi\rho_{s*})^{1/3}$, and they were $R_*^* = 2.49$−$6.95$ (0.85−2.37 nm) at $T = (0.731$−$0.896)T_m$, respectively. To a first approximation, $R_*$ is a linear function of the inverse temperature $1/\Delta T$.

In the region of moderate supercoolings, our results for $n_*(T)$ agree with the data of Espinosa et al.,[36] who also used the seeding method to study LJ liquid crystallization. At a temperature $T = 0.864T_m$, our value $n_* = 608$ particles is only 4% higher than their $n_* = 585$. In the region of high supercoolings, the obtained $n_*(T)$ agree with independent calculations using the MFPT method.[18,92] At the lowest temperature studied, $T = 0.731T_m$, we obtained $n_* = 65$, whereas the MFPT yielded $n_* = 58(14)$.[18]

In the whole temperature range studied, the obtained values $n_*(T)$ are approximately two times higher than the values reported by Bai and Li.[34,35] Such discrepancy can be explained by the poorer statistics of nucleation events in those earlier MD calculations and by differences in the seed introduction procedures. In accordance with eq 12, a 2-fold change of $n_*$ leads to a change of $\gamma_e$ by 26%.

The stable phase of the LJ crystal has the fcc structure. Therefore, the effective number of atoms per unit cell is 4.



DOI: 10.1021/acs.jpcc.8b10637
J. Phys. Chem. C 2018, 122, 28884−28894

Smoothly extrapolating $n_*(T)$ to deeper supercoolings leads to $n = 4$ at $T \approx 0.4T_m$ (insert in Figure 2). As a critical nucleus cannot be smaller than a single unit cell, the CNT is no longer valid below this temperature.

To check the sensitivity of the MD simulation procedure to the imposed conditions, we carried out four additional tests of the seeding method at $T = 0.809T_m$, with 50 independent runs for each assumption:

**Finite-Size Effect.** Observation of the evolutions of crystalline seeds, $n = 207$, introduced into supercooled liquid systems containing $N = 3 \times 10^3$, $3 \times 10^4$, $3 \times 10^5$ particles, showed that the size of the critical nucleus does not depend significantly on the box size. At the same time, a decrease of $E_{pot}$ of 1% occurred approximately twice as fast in the system with $N = 3 \times 10^4$ than with $N = 3 \times 10^5$. This phenomenon was observed earlier and treated as a time-lag[35] due to differences in the thermal fluctuation magnitudes in systems of different sizes. We consider this effect as an artifact of the NpT ensemble.[93]

**Seed Density.** In the investigated temperature range, the crystal seed and liquid phase densities are related by $\rho/s_*\rho = 1.11(1)$. We have found that a decrease/increase in the initial value of $\rho s_*$ by 11% (at fixed $T$ and $R_*$) did not lead to a significant change in the probability of crystallization (at least with the seeding and equilibration strategy used here). In accordance with eq 12, a deviation of $\rho_{s*}$ by 11% leads to changes in the value of $\gamma_e$ by 7%.

**Seed Temperature.** In accordance with the CNT, the temperatures of the metastable and competing phases are assumed to be equal. Alternative theories of crystallization (e.g., based on the generalized Gibbs' approach)[94,95] allow for their difference. The temperatures of the crystal seeds ranged from $T = 0.728T_m$ to $0.890T_m$. This corresponds to a maximum deviation between the seed and its surrounding liquid temperature by 10%. We found that one-percent difference in temperatures did not significantly affect the probability of growth/decay of seeds. The decrease (increase) in seed temperature by 10% has always led to their growth (decay).

**Seed Structure.** A significant influence in the structure of crystal seeds on the crystallization kinetics was previously detected.[17,37−40,57] However, spherical ice seeds having different (cubic, hexagonal) structures were critical at the same temperature and had equal values of interfacial free energies, calculated via the seeding approach.[48] In this study, while preserving both the seed radius and its density, nuclei with hcp, fcc, and bcc crystal lattice were introduced. The enthalpies of inserted crystals were $H^{(hcp)} < H^{(fcc)} < H^{(bcc)}$. We found that any supercooled liquid containing bcc or hcp seeds with $n = 207$, always crystallized at $T = 0.809T_m$. As the fcc seed of the same size was critical sized, consequently, the critical sizes of bcc or hcp seeds are smaller than that of the fcc. Hence, according to eq 12, the interfacial free energy of the fcc nucleus is the largest. A study of a possible martensitic transformation during the evolution of the seed was not carried out in this work.

Summarizing, we conclude that the results of the seeding procedure are indeed sensitive to the starting conditions of the parameters of the embedded crystalline seed, such as the temperature and structure, but not to their density, at least for small crystalline seeds containing only a few hundred particles. This topic warrants further studies because the critical nucleus is determined not only by its size but also by its shape and structure, that is, crystal nucleation can occur along different pathways.[57,92,96] However, significant box finite-size effects in liquid crystallization by the seeding method were not detected.

**Thermodynamic Driving Force.** The expression 3 for $\Delta\mu$, often used in molecular dynamics simulations and in experimental studies of spontaneous crystallization for evaluation of $\gamma_e$, is strictly valid for small supercoolings or when the specific heats of the supercooled liquid and crystal phases are similar. Following ref 18, the driving force of crystallization, $\Delta\mu(T)$, was calculated by eq 13 using two parameters $p_{s*}$ and $\rho_{s*}$ determined from the simulations. The discrepancy between the values of $\Delta\mu$ obtained by eqs 3 and 13, reached 15% at $T = 0.7T_m$.[18] We found that among the eqs 3−6, expression 5 best describes the $\Delta\mu(T)$ for LJ obtained from MD data by eq 13, with a difference not exceeding 2%.

**Interfacial Free Energy.** The effective interfacial free energy of the critical crystal nucleus/supercooled liquid, $\gamma_e$, calculated by eqs 12 and 13 based on MD data for $p(T)s_*$, $\rho(T)s_*$, and $n_*(T)$ is shown in Figure 3. The obtained values of

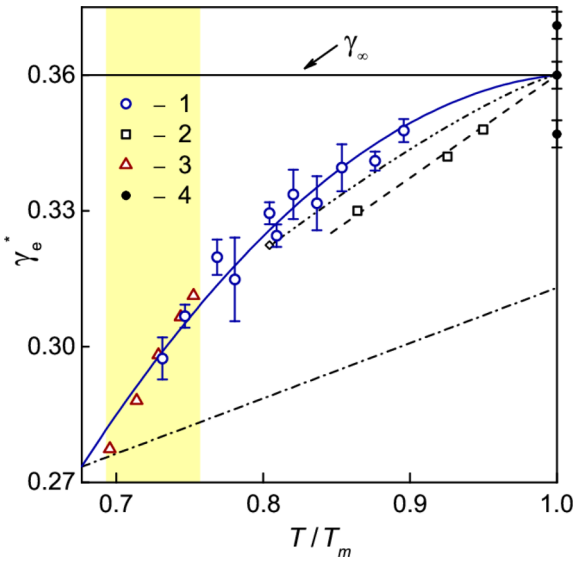


**Figure 3.** Effective interfacial free energy of the critical crystal nucleus/supercooled liquid $\gamma_e$ versus supercooling $T/T_m$ at $p = 0$: 1, calculation by eqs 12 and 13 from MD data of $n_*$, $p_{s*}$, and $\rho_{s*}$; 2, data of Espinosa et al.,[36] which were linearly approximated by the dashed line; 3, calculation by eqs 1, 7, 13 by the MD data for $J$, $\mathcal{D}_*$, $Z_*$, $\rho$, $T$, and $p_{s*}$;[18] 4, values of $\gamma_\infty$ for three flat crystallographic surfaces (110), (110), and (111),[77] and the corresponding orientation-averaged value is indicated by the horizontal line. The solid line is the smooth approximation of our data and refs.[18,77] The dash-dotted line refers to the data of Bai and Li.[35] The dash-dot-dot line is the interfacial free energy at the metastable extension of the melting line ($p < 0$): $\gamma_\infty^* = 0.322 + 0.522 \times (T^*-0.497)^{1.246}$.[100] The temperature range of a homogeneous crystallization study by a brute-force MD[18] is highlighted in yellow.

$\gamma_e(T)$ are larger than the values of refs 35 and 36. In the investigated range of state parameters at $p = 0$, values $\gamma_e$ are smaller than for a flat interface, $\gamma_\infty$, and decrease monotonically with increasing supercooling, reaching $0.83\gamma_\infty$ at $T = 0.73T_m$.

The decrease of $\gamma_e$ with increasing supercooling during the isobaric approach to the metastable region was predicted theoretically in refs 97 and 98. The values of $\gamma_e$ obtained by the seeding method at high supercoolings agree with the result of the CNT calculations by eqs 1, 7, and 13 using MD data,[18]


DOI: 10.1021/acs.jpcc.8b10637
J. Phys. Chem. C 2018, 122, 28884−28894

where $\gamma_e$ was considered as the single "free" parameter. Finally, our data on $\gamma_e$ extrapolate well to its value for a flat interface $\gamma_\infty$.[77]

It was previously established[19,99] that, at a fixed temperature, the critical crystal nucleus/supercooled liquid interface free energy, $\gamma_e$, is higher than that of a flat interface, $\gamma_\infty$. Figure 3 shows that the relation $\gamma_e(T,p = 0) > \gamma_\infty(T,p < 0)$ is also satisfied. Here we use the temperature dependence for $\gamma_\infty(T)$ at $p < 0$ proposed in ref 100.

With the use of the values of $\gamma_e$ and $ps_*$, the work of formation of the critical nucleus, $W_*$, was calculated from formulas 1 and 13. The reduced value of the activation barrier $W_*/k_BT$ varies from 17.0(4) at $T = 0.731T_m$ to 127(1) at $T = 0.896T_m$. The use of eq 3 for $\Delta\mu$ leads to $W_*/k_BT = 12.7(2)$ and 117(1), respectively. That is, the difference of $W_*/k_BT$ using $\Delta\mu$ obtained by eq 13 using the MD data, and according to formula 3, reaches 25% in the region of deep supercoolings. The value $W_*/k_BT$ at $T = 0.731T_m$, which was calculated earlier from the MD data of $\rho$, $\mathcal{D}_*$, $Z_*$ and $J$ as $W_*/k_BT = \ln(\rho\mathcal{D}_*Z_*/J)$, is 17.1,[18] which coincides with our current estimate. At $T = 0.8T_m$ and $p = 0.25$ kbar, the calculated value of $W_*/k_BT$ by the method of metadynamics equals 35(2).[101] This result is similar to our estimation $W_*/k_BT = 37.2(4)$ at the same supercooling at $p = 0$.

We also calculated the Zeldovich factor, $Z_*$, using the data for $W_*$ and $n_*$ in eq 8. The value $Z_*$ increases from 0.003 at $T = 0.896T_m$ to 0.021 at $T = 0.731T_m$, whereas the $Z_*$ obtained independently by the MFPT method at $T = 0.728T_m$ is 0.020(3).[18]

**Transport Coefficient at the Nucleus/Liquid Interface.** To test the CNT, we also need the transport coefficient at the liquid/nucleus interface, $\mathcal{D}_*$. Following ref 102, $\mathcal{D}_*$ was obtained from the MD simulations by

$$D_* = \frac{1}{2}\frac{\langle \Delta n^2(t)\rangle}{t} \tag{14}$$

where $\Delta n(t) = n(t) - n_*$ is the change in the number of particles in the crystalline seed over time. This is the effective attachment coefficient for crystalline nucleus growth rates. During 20 ps after the implementation, every 0.5 ps, the size of the nucleus $n(t)$ was calculated by analyzing the particle configurations using the q6 method. We carried out 50 independent evolutions of the embedded critical crystal $n(t)$ in 6 thermodynamic states. The slope of the time dependence of $\langle[n(t) - n_*]^2\rangle$ at each temperature determined the value of $\mathcal{D}_*$. The result from the seeded simulations is that $\mathcal{D}_*(T)$ has an exponential behavior. Supplementing with data of spontaneous nucleation of ref 18, it changes by 2 orders of magnitude in the temperature range $T = (0.728–0.896)T_m$ (Figure 4). The current values of $\mathcal{D}_*$ agree well with the data of refs 18 and 92 in the region of high supercoolings but exceed the values of ref 36 by 1 order of magnitude.

Using the MD data for $\mathcal{D}_*$ and $n_*$ in eq 10, the activation energy $E(T)$ was estimated. In the temperature range $T = (0.731–0.896)T_m$, $E$ increases with supercooling from 0.5 $k_BT$ to 1.4 $k_BT$. Note that for each inserted seed, the number of surface atoms $i_*$ in eq 10 was calculated separately. For such small spherical nuclei studied here, whose diameters do not exceed 5 nm, the ratio $i_*/n_*$ varies from 0.35 to 0.72. While for larger clusters, of hundreds of nanometers, the number of surface atoms is less than 5% of the total number.[103]

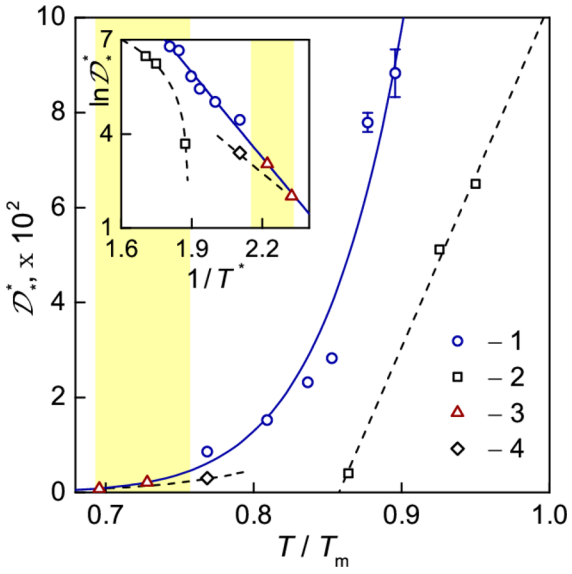


**Figure 4.** Transport coefficient of interfacial atomic attachment, $\mathcal{D}_*$, versus temperature along the zero isobar, calculated by eq 14: 1, current results; 2, data of Espinosa et al.,[36] which were linearly approximated by the dashed line; 3, data of Baidakov and Tipeev;[18] 4, data of Malek et al.,[92] obtained for a system with $N = 600$ particles. The solid line is an approximation by eq 10 of the MD data of $\mathcal{D}_*$. The temperature range of a homogeneous crystallization study by a brute-force MD[18] is shown in yellow. Inset: logarithm of $\mathcal{D}_*$ as a function of the inverse temperature.

Thus, for supercooling a LJ liquid in the range $T = (0.731–0.896)T_m$ at $p = 0$, there is a significant superiority of the thermodynamic barrier, $W_*/k_BT = 12.7–127$, over the kinetic one, $E/k_BT = 0.5–1.4$. Even at the maximum attainable supercooling of an unseeded LJ liquid $T = 0.696T_m$, corresponding to a nucleation rate of $J \approx 10^{34}$ s$^{-1}$ m$^{-3}$, achieved in the system $N = 2048$ after a cooling rate $\approx 10^{11}$ K/s, the work of forming a critical nucleus is $W_* = 11.7\ k_BT$.[18] Moreover, the kinetic activation energy at this same thermodynamic state, estimated from data of ref 18, is only $E \approx 2.2\ k_BT$. Consequently, for all supercoolings, down to $T \approx 0.7T_m$, the kinetic barrier was lower than the thermodynamic barrier [i.e., $E(T) < W_*(T)$]. On the other hand, it was shown recently,[42,43,104] that for the good glass-forming alloy $Cu_{50}Zr_{50}$, the opposite situation takes place, $E > W_*$, that is, this high kinetic barrier does not allow observation of homogeneous, spontaneous nucleation. In this case, the seeding method would be especially useful in accelerating crystallization.

**Comparing the Calculated Nucleation Rates with Directly Determined Values.** Figure 5 shows the temperature dependence of the calculated nucleation rate, $J$, in the supercooled liquid at $p = 0$. The values of $J$ were obtained by eq 9, using eq 13 for $\Delta\mu$, and the MD results for $T_m$, $T$, $\rho$, $\rho_{s*}$, $p_{s*}$, $n_*$, and $\mathcal{D}_*$. For the thermodynamic states under investigation, $T = (0.731–0.896)T_m$, the value of $J$ changed from $J = 2 \times 10^{32}$ s$^{-1}$ m$^{-3}$ ($J^* = 2 \times 10^{-8}$) to $1 \times 10^{-15}$ s$^{-1}$ m$^{-3}$ ($J^* = 1 \times 10^{-55}$). Direct calculation by the mean lifetime method at $T = 0.728T_m$ yielded $J^* = 1.6(1) \times 10^{-818}$ in excellent agreement with the present calculations from the seeding method ($J^* = 2 \times 10^{-8}$). This value also agrees very well with a recent independent calculation by the forward flux sampling technique, which yielded $J^* = 1.9(6) \times 10^{-8}$.[105] At $T = 0.744T_m$, the mean lifetime method yielded $J^* = 1.0(1) \times$


DOI: 10.1021/acs.jpcc.8b10637
J. Phys. Chem. C 2018, 122, 28884–28894

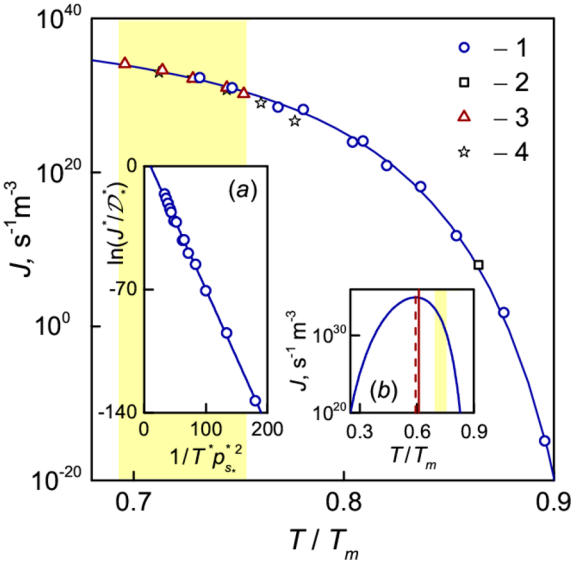


**Figure 5.** Temperature dependence of the nucleation rate, $J$, at $p = 0$: 1, current results; 2, data of Espinosa et al.;[36] 3, data of Baidakov and Tipeev;[18] 4, data from Haji-Akbari.[105] The solid line is the theoretical calculation of $J(T)$ by eqs 1, 3, 7, assuming $\gamma_e(T) = \gamma_\infty$ and the theoretical value of the pre-exponential. The temperature range of a homogeneous crystallization study by a brute-force MD[18] is shown in yellow. Insets: (a) logarithm of $J/\mathcal{D}_*$ as a function of $T^{-1}\, p_{s*}^{-2}$; (b) nucleation rate as a function of $T/T_m$. The vertical dashed line indicates the position of the maximum. The solid line indicates the position, $T/T_m \approx 0.61$, where the CNT breaks down, $W_*/k_BT \approx 1$.

$10^{-9}$,[18] which is in remarkable agreement with the result of the seeding method at $T = 0.747T_m$: $J^* = 1.1(3) \times 10^{-9}$.

Using the expressions 3−6 to estimate $\Delta\mu$ in eq 9 leads to maximum discrepancy between calculated values of $J$ only 2 orders of magnitude at $T = 0.731T_m$ and 6 orders at $T = 0.896T_m$. The nucleation rates and other calculated crystallization parameters are shown in Table 1 for three temperatures among the 11 under investigation.

To compare our results with the same type of analysis that experimentalists normally do, we plotted the logarithm of $(J/\mathcal{D}_*)$ versus $T^{-1}\, p_{s*}^{-2}$, shown in Figure 5a. This dependence is almost linear over many orders of magnitude. By approximating that curve by a linear function, according to eqs 1, 7, 13, we obtained $\langle\rho^* Z_*\rangle = 6(5) \times 10^3$ and an average interfacial free energy $\langle\gamma_e^*\rangle = 0.361(2)$. This value of $\langle\gamma_e\rangle$ is equal to $\gamma_\infty$, as often suggested in the CNT. In this case, the theoretical factor $\langle\rho^* Z_*\rangle$, determined as the $y$-axis intercept of the plot, is 6 orders of magnitude higher than the average theoretical value resulting from the MD simulation, $\langle\rho^* Z_*\rangle = 0.01$.

**Table 1. Crystallization Parameters at $p = 0$**

| quantity | temperature | | |
|---|---|---|---|
| | $T^* = 0.452(3)$ | $T^* = 0.500(1)$ | $T^* = 0.5535(5)$ |
| $T/T_m$ | 0.731(5) | 0.809(2) | 0.896(1) |
| $\rho^*$ | 0.904 | 0.884 | 0.860 |
| $\rho_{s*}^*$ | 0.995(1) | 0.982(1) | 0.967(1) |
| $p_{s*}^*$ | 0.239(4) | 0.176(1) | 0.100(1) |
| $n_*$ | 64 | 207 | 1357 |
| $R_*$, nm | 0.85 | 1.26 | 2.37 |
| $\Delta\mu/k_BT$, eq 3 | 0.61(2) | 0.395(4) | 0.195(2) |
| $\Delta\mu/k_BT$, eq 13 | 0.53(1) | 0.358(3) | 0.187(2) |
| $E/k_BT$ | 1.4(2) | 0.52(3) | 0.48(6) |
| $W_*/k_BT$ | 17.0(4) | 37.0(4) | 127(1) |
| $Z_*$ | 0.021 | 0.010 | 0.003 |
| D** | 27(4) | 152(4) | 880(50) |
| $\gamma_e^*$ | 0.297(5) | 0.325(2) | 0.348(3) |
| $J^*$, eqs 9 and 13 | $2 \times 10^{-8}$ | $1 \times 10^{-16}$ | $1 \times 10^{-55}$ |
| $J^*$ (MD)[18] | $1.6 \times 10^{-8}$ | – | – |

We also compared the results of the simulations with those which would be obtained with the upper, eq 3, and lower bound, eq 4, expressions for the driving force, $\Delta\mu$, which are widely used by authors of simulation works and experimentalists that do not have the actual value of $\Delta\mu$. Using the expression 3 for $\Delta\mu$ yielded $\langle\rho^* Z_*\rangle \approx 1$ and $\langle\gamma_e^*\rangle = 0.364$. Using the expression 4 for $\Delta\mu$ yielded $\langle\rho^* Z_*\rangle \approx 10^7$ and $\langle\gamma_e^*\rangle = 0.350$.

Finally, by using the macroscopic value of $\langle\gamma_e\rangle \approx \gamma_\infty$ and the fitted value of $\langle\rho^* Z_*\rangle = 6(5) \times 10^3$ in eq 7, we plotted the nucleation rate curve in a wide range of supercoolings. The resulting $J(T)$ has the expected dome shape with a maximum at $T = 0.59T_m$, which corresponds to $J = 1.1 \times 10^{35}$ s$^{-1}$ m$^{-3}$ (Figure 5b). This position of the maximum corresponds to a critical nucleus containing $n_* = 11$ particles. However, note that by extrapolating the data ref 99 on the height of the thermodynamic barrier, $W_*(T)$, we estimated that this barrier becomes $\approx 1 \times k_BT$ already at $T \approx 0.61T_m$. Therefore, the CNT is no longer valid for this LJ liquid at such deep supercooling.

In accordance with eq 7, with increasing supercooling, the steady-state nucleation rate, $J$, is determined by the interplay between the increase of the exponential term, determined by the work of critical nucleus formation, $W_*$, and the decrease of the transport coefficient at the supercooled liquid/crystal interface, $\mathcal{D}_*$. This interplay determines the magnitude and location of the maximum homogeneous nucleation rate, which for real, experimental glass-forming substances is near their laboratory glass transition temperature, which are also located at $(0.5-0.6)T_m$.[106,107] For a LJ liquid, decreasing the temperature from $0.896T_m$ to $0.731T_m$, the height of the thermodynamic barrier decreases from 127 to 17 $k_BT$, which changes $\exp(-W_*/k_BT)$ by 48 decades, whereas the transport term, $\mathcal{D}_*$, decreases only 33 times. Such changes lead to a very sharp increase in the nucleation rate of 47 orders of magnitude in the indicated temperature range. Taken *in toto*, the present results for seeded nucleation, good agreement of nucleation rates calculated theoretically by CNT and via computer simulations, corroborate those established earlier for spontaneous, homogeneous crystallization of a highly supercooled LJ liquid, $T < 0.73T_m$.[18,99,108]

## IV. SUMMARY AND CONCLUSIONS

We carried out thorough molecular dynamics simulations of the crystallization kinetics of a fast quenched Lennard-Jones liquid at constant (zero) pressure, at 11 supercoolings. We used the seeding method to determine the number of particles in the critical crystalline nuclei, which was $n_* = 64-1357$, corresponding to calculated spherical radii of $R_* = (0.9-2.4)$ nm in the supercooling range $T = (0.731-0.896)T_m$. We also obtained the atomic transport coefficient at the liquid/nucleus interface, $\mathcal{D}_*$, the density and pressure in the critical crystal nuclei.



DOI: 10.1021/acs.jpcc.8b10637
J. Phys. Chem. C 2018, 122, 28884−28894

We then calculated by CNT the effective interfacial free energy of the critical crystal nucleus/supercooled liquid, $\gamma_e$, using the physical parameters $n_*$ and $\Delta\mu$ resulting from the simulations. For the investigated range of state parameters, the obtained values of $\gamma_e$ are smaller than that of the flat, macroscopic crystal/liquid interface, $\gamma_\infty$, and decrease with increasing supercooling. In general, we found a good agreement between the values of $n_*$, $W_*$, and $\gamma_e$ obtained here by the seeding method with previous simulations of spontaneous nucleation in the region of high metastability, $T \approx 0.73T_m$.

For the range of supercoolings studied, the theoretically calculated values of the nucleation rate varied from $J = 1 \times 10^{-15}$ s$^{-1}$ m$^{-3}$ to $2 \times 10^{32}$ s$^{-1}$ m$^{-3}$. The most important finding of this research is that the calculated nucleation rate at one supercooling agrees rather well with a direct MD determination. This result corroborates the validity of the CNT for this LJ liquid and contrasts with the colossal discrepancies of 30−55 orders of magnitude between the theoretical and experimental nucleation rates in inorganic glass formers.

We propose that the key factor to explain the ability of the CNT in describing nucleation rates is the use of the correct parameters $n_*(T)$, $\Delta\mu(T)$, and $\mathcal{D}_*(T)$, directly obtained from the simulations, instead of frequently used approximations: (fitted) average interfacial energy, calculated $\Delta\mu$, and other approximations, such as viscosity or nucleation time-lags, for the transport term in the analysis of experimental nucleation rates in glass-forming substances.

## AUTHOR INFORMATION


### Corresponding Author

*E-mail: azattipeev@gmail.com.

### ORCID

Azat O. Tipeev: 0000-0002-6939-7339


### Notes

The authors declare no competing financial interest.

## ACKNOWLEDGMENTS

A.O.T. acknowledges the São Paulo Research Foundation (FAPESP) for his postdoctoral fellowship (Grant 2017/08350-1). E.D.Z. and J.P.R. would also like to thank FAPESP (contract CEPID 2013/07793-6) for the financial support of this research. Finally, we appreciate the critical comments of Alexander Abyzov. All MD results were obtained using the supercomputer ≪Terra≫ from the Physics Department, Federal University of São Carlos, Brazil.

## REFERENCES


(1) Gibbs, J. W. *Scientific Papers, Vol. I, II*; Longmans: London, 1906.

(2) Kelton, K. F.; Greer, A. L. *Nucleation in Condensed Matter: Applications in Materials and Biology*, 1st ed.; Pergamon: United Kingdom, 2010.

(3) Skripov, V. P.; Koverda, V. P. *Spontaneous Crystallization of Supercooled Liquids*; Nauka: Moscow, 1984.

(4) Kelton, K. F. Crystal Nucleation in Liquids and Glasses. *Solid State Phys.* **1991**, *45*, 75−177.

(5) Hoffman, J. D. Thermodynamic Driving Force in Nucleation and Growth Processes. *J. Chem. Phys.* **1958**, *29*, 1192−1193.

(6) Thompson, C. V.; Spaepen, F. Homogeneous Crystal Nucleation in Binary Metallic Melts. *Acta Metall.* **1979**, *27*, 1855−1859.

(7) Singh, H. B.; Holz, A. Stability Limit of Supercooled Liquids. *Solid State Commun.* **1983**, *45*, 985−988.

(8) Zeldovich, Ya. B. On the Theory of New Phase Formation. *Zh. Eksp. Teor. Fiz.* **1942**, *12*, 525−538.

(9) Turnbull, D.; Fisher, J. C. Rate of Nucleation in Condensed Systems. *J. Chem. Phys.* **1949**, *17*, 71−73.

(10) Fokin, V. M.; Zanotto, E. D.; Yuritsyn, N. S.; Schmelzer, J. W. P. Homogeneous Crystal Nucleation in Silicate Glasses: A 40 Years Perspective. *J. Non-Cryst. Solids* **2006**, *352*, 2681−2714.

(11) Sosso, G. C.; Chen, J.; Cox, S. J.; Fitzner, M.; Pedevilla, P.; Zen, A.; Michaelides, A. Crystal Nucleation in Liquids: Open Questions and Future Challenges in Molecular Dynamics Simulations. *Chem. Rev.* **2016**, *116*, 7078−7116.

(12) Turnbull, D.; Cech, R. E. Microscopic Observation of the Solidification of Small Metal Droplets. *J. Appl. Phys.* **1950**, *21*, 804−810.

(13) Gupta, P. K.; Cassar, D. R.; Zanotto, E. D. Role of Dynamic Heterogeneities in Crystal Nucleation Kinetics in an Oxide Supercooled Liquid. *J. Chem. Phys.* **2016**, *145*, 211920.

(14) Abyzov, A. S.; Fokin, V. M.; Rodrigues, A. M.; Zanotto, E. D.; Schmelzer, J. W. P. The Effect of Elastic Stresses on the Thermodynamic Barrier for Crystal Nucleation. *J. Non-Cryst. Solids* **2016**, *432*, 325−333.

(15) Yau, S.-T.; Vekilov, P. G. Quasi-planar Nucleus Structure in Apoferritin Crystallization. *Nature* **2000**, *406*, 494−497.

(16) Gasser, U.; Weeks, E. R.; Schofield, A.; Pusey, P. N.; Weitz, D. A. Real-space Imaging of Nucleation and Growth in Colloidal Crystallization. *Science* **2001**, *292*, 258−262.

(17) Schöpe, H. J.; Wette, P. Seed- and Wall-Induced Heterogeneous Nucleation in Charged Colloidal Model Systems under Microgravity. *Phys. Rev. E* **2011**, *83*, 051405.

(18) Baidakov, V. G.; Tipeev, A. O. Crystal Nucleation and the Solid-Liquid Interfacial Free Energy. *J. Chem. Phys.* **2012**, *136*, 074510.

(19) Baidakov, V. G.; Tipeev, A. O.; Bobrov, K. S.; Ionov, G. V. Crystal Nucleation Rate Isotherms in Lennard-Jones Liquids. *J. Chem. Phys.* **2010**, *132*, 234505.

(20) Torrie, G. M.; Valleau, J. P. Monte Carlo Free Energy Estimates Using Non-Boltzmann Sampling: Application to the Sub-Critical Lennard-Jones Fluid. *Chem. Phys. Lett.* **1974**, *28*, 578−581.

(21) Laio, A.; Parrinello, M. Escaping Free-Energy Minima. *Proc. Natl. Acad. Sci. U. S. A.* **2002**, *99*, 12562−12566.

(22) van Erp, T. S.; Moroni, D.; Bolhuis, P. G. A Novel Path Sampling Method for the Calculation of Rate Constants. *J. Chem. Phys.* **2003**, *118*, 7762−7774.

(23) Allen, R. J.; Frenkel, D.; ten Wolde, P. R. Forward Flux Sampling-Type Schemes for Simulating Rare Events: Efficiency Analysis. *J. Chem. Phys.* **2006**, *124*, 194111.

(24) Dellago, C.; Bolhuis, P. G.; Chandler, D. Efficient Transition Path Sampling: Application to Lennard-Jones Cluster Rearrangements. *J. Chem. Phys.* **1998**, *108*, 9236−9245.

(25) Zhou, H.; Lin, X.; Wang, M.; Huang, W. Calculation of Solid-Liquid Interfacial Free Energy of Cu by Two Different Methods. *J. Cryst. Growth* **2013**, *377*, 107−111.

(26) Bergfors, T. Seeds to Crystals. *J. Struct. Biol.* **2003**, *142*, 66−76.

(27) Parambil, J. V.; Heng, J. Y. Y. Seeding in Crystallisation. In *Engineering Crystallography: From Molecule to Crystal to Functional Form*; Roberts, K.; Docherty, R.; Tamura, R., Eds.; Springer: Dordrecht, 2017, pp 235−245.

(28) Bording, J. K.; Taftø, J. Molecular-Dynamics Simulation of Growth of Nanocrystals in an Amorphous Matrix. *Phys. Rev. B: Condens. Matter Mater. Phys.* **2000**, *62*, 8098−8103.

(29) Pan, B. C.; Biswas, R. Structure and Simulation of Hydrogenated Nanocrystalline Silicon. *J. Appl. Phys.* **2004**, *96*, 6247−6252.

(30) Mattoni, A.; Colombo, L. Nonuniform Growth of Embedded Silicon Nanocrystals in an Amorphous Matrix. *Phys. Rev. Lett.* **2007**, *99*, 205501.

(31) Wu, L. K.; Li, Q. L.; Xu, B.; Liu, W. Calculation of Solid-Liquid Interfacial Free Energy of Silicon Based on Classical Nucleation Theory. *J. Mater. Res.* **2016**, *31*, 3649−3656.




DOI: 10.1021/acs.jpcc.8b10637
J. Phys. Chem. C 2018, 122, 28884−28894

(32) Cacciuto, A.; Auer, S.; Frenkel, D. Onset of Heterogeneous Crystal Nucleation in Colloidal Suspensions. *Nature* **2004**, *428*, 404−406.
(33) Browning, A. R.; Doherty, M. F.; Fredrickson, G. H. Nucleation and Polymorph Selection in a Model Colloidal Fluid. *Phys. Rev. E* **2008**, *77*, 041604.
(34) Bai, X.-M.; Li, M. Test of Classical Nucleation Theory via Molecular-Dynamics Simulation. *J. Chem. Phys.* **2005**, *122*, 224510.
(35) Bai, X.-M.; Li, M. Calculation of Solid-Liquid Interfacial Free Energy: A Classical Nucleation Theory Based Approach. *J. Chem. Phys.* **2006**, *124*, 124707.
(36) Espinosa, J. R.; Vega, C.; Valeriani, C.; Sanz, E. Seeding Approach to Crystal Nucleation. *J. Chem. Phys.* **2016**, *144*, 034501.
(37) Jungblut, S.; Dellago, C. Heterogeneous Crystallization on Tiny Clusters. *Europhys. Lett.* **2011**, *96*, 56006.
(38) Jungblut, S.; Dellago, C. Crystallization on Prestructured Seeds. *Phys. Rev. E* **2013**, *87*, 012305.
(39) Jungblut, S.; Dellago, C. On the Reaction Coordinate for Seeded Crystallization. *Mol. Phys.* **2015**, *113*, 2735−2741.
(40) Jungblut, S.; Dellago, C. Heterogeneous Crystallization on Pairs of Pre-Structured Seeds. *J. Phys. Chem. B* **2016**, *120*, 9230−9239.
(41) Suh, D.; Yasuoka, K. Heterogeneous Cavitation and Crystallisation with an Impurity by Molecular Dynamics. *Mol. Simul.* **2018**, *44*, 530−533.
(42) Sun, Y.; Song, H.; Zhang, F.; Yang, L.; Ye, Z.; Mendelev, M. I.; Wang, C.-Z.; Ho, K.-M. Overcoming the Time Limitation in Molecular Dynamics Simulation of Crystal Nucleation: A Persistent-Embryo Approach. *Phys. Rev. Lett.* **2018**, *120*, 085703.
(43) Yang, L. Structures and Dynamics Investigation of Phase Selection in Metallic Alloy Systems. PhD thesis, Iowa State University, 2018.
(44) Hashimoto, R.; Shibuta, Y.; Suzuki, T. Estimation of Solid-liquid Interfacial Energy from Gibbs-Thomson Effect: A Molecular Dynamics Study. *ISIJ Int.* **2011**, *51*, 1664−1667.
(45) Pereyra, R. G.; Szleifer, I.; Carignano, M. A. Temperature Dependence of Ice Critical Nucleus Size. *J. Chem. Phys.* **2011**, *135*, 034508.
(46) Sanz, E.; Vega, C.; Espinosa, J. R.; Caballero-Bernal, R.; Abascal, J. L. F.; Valeriani, C. Homogeneous Ice Nucleation at Moderate Supercooling from Molecular Simulation. *J. Am. Chem. Soc.* **2013**, *135*, 15008−15017.
(47) Espinosa, J. R.; Sanz, E.; Valeriani, C.; Vega, C. Homogeneous Ice Nucleation Evaluated for Several Water Models. *J. Chem. Phys.* **2014**, *141*, 18C529.
(48) Zaragoza, A.; Conde, M. M.; Espinosa, J. R.; Valeriani, C.; Vega, C.; Sanz, E. Competition between Ices Ih and Ic in Homogeneous Water Freezing. *J. Chem. Phys.* **2015**, *143*, 134504.
(49) Espinosa, J. R.; Zaragoza, A.; Rosales-Pelaez, P.; Navarro, C.; Valeriani, C.; Vega, C.; Sanz, E. Interfacial Free Energy as the Key to the Pressure-Induced Deceleration of Ice Nucleation. *Phys. Rev. Lett.* **2016**, *117*, 135702.
(50) Espinosa, J. R.; Navarro, C.; Sanz, E.; Valeriani, C.; Vega, C. On the Time Required to Freeze Water. *J. Chem. Phys.* **2016**, *145*, 211922.
(51) Espinosa, J. R.; Soria, G. D.; Ramirez, J.; Valeriani, C.; Vega, C.; Sanz, E. Role of Salt, Pressure, and Water Activity on Homogeneous Ice Nucleation. *J. Phys. Chem. Lett.* **2017**, *8*, 4486−4491.
(52) Lupi, L.; Hudait, A.; Peters, B.; Grünwald, M.; Gotchy Mullen, R.; Nguyen, A. H.; Molinero, V. Role of Stacking Disorder in Ice Nucleation. *Nature* **2017**, *551*, 218−222.
(53) Soria, G. D.; Espinosa, J. R.; Ramirez, J.; Valeriani, C.; Vega, C.; Sanz, E. A Simulation Study of Homogeneous Ice Nucleation in Supercooled Salty Water. *J. Chem. Phys.* **2018**, *148*, 222811.
(54) Pedevilla, P.; Fitzner, M.; Sosso, G. C.; Michaelides, A. Heterogeneous Seeded Molecular Dynamics as a Tool to Probe the Ice Nucleating Ability of Crystalline Surfaces. *J. Chem. Phys.* **2018**, *149*, 072327.
(55) Zaragoza, A.; Espinosa, J. R.; Ramos, R.; Cobos, J. A.; Aragones, J. L.; Vega, C.; Sanz, E.; Ramírez, J.; Valeriani, C. Phase Boundaries, Nucleation Rates and Speed of Crystal Growth of the Water-to-Ice Transition under an Electric Field: a Simulation Study. *J. Phys.: Condens. Matter* **2018**, *30*, 174002.
(56) Espinosa, J. R.; Vega, C.; Sanz, E. Homogeneous Ice Nucleation Rate in Water Droplets. *J. Phys. Chem. C* **2018**, *122*, 22892−22896.
(57) Hermes, M.; Vermolen, E. C. M.; Leunissen, M. E.; Vossen, D. L. J.; van Oostrum, P. D. J.; Dijkstra, M.; van Blaaderen, A. Nucleation of Colloidal Crystals on Configurable Seed Structures. *Soft Matter* **2011**, *7*, 4623−4628.
(58) Allahyarov, E.; Sandomirski, K.; Egelhaaf, S. U.; Löwen, H. Crystallization Seeds Favour Crystallization only during Initial Growth. *Nat. Commun.* **2015**, *6*, 7110.
(59) Bommineni, P. K.; Punnathanam, S. N. Molecular Simulation of Homogeneous Crystal Nucleation of AB2 Solid Phase From a Binary Hard Sphere Mixture. *J. Chem. Phys.* **2017**, *147*, 064504.
(60) Sharma, A. K.; Escobedo, F. A. Nucleus-Size Pinning for Determination of Nucleation Free-Energy Barriers and Nucleus Geometry. *J. Chem. Phys.* **2018**, *148*, 184104.
(61) Richard, D.; Speck, T. Crystallization of Hard Spheres Revisited. II. Thermodynamic Modeling, Nucleation Work, and the Surface of Tension. *J. Chem. Phys.* **2018**, *148*, 224102.
(62) Kalikka, J.; Akola, J.; Larrucea, J.; Jones, R. O. Nucleus-Driven Crystallization of Amorphous $Ge_2Sb_2Te_5$: A Density Functional Study. *Phys. Rev. B: Condens. Matter Mater. Phys.* **2012**, *86*, 144113.
(63) Knott, B. C.; Molinero, V.; Doherty, M. F.; Peters, B. Homogeneous Nucleation of Methane Hydrates: Unrealistic under Realistic Conditions. *J. Am. Chem. Soc.* **2012**, *134*, 19544−19547.
(64) Zepeda-Ruiz, L. A.; Sadigh, B.; Chernov, A. A.; Haxhimali, T.; Samanta, A.; Oppelstrup, T.; Hamel, S.; Benedict, L. X.; Belof, J. L. Extraction of Effective Solid-Liquid Interfacial Free Energies for Full 3D Solid Crystallites from equilibrium MD Simulations. *J. Chem. Phys.* **2017**, *147*, 194704.
(65) Watanabe, Y.; Shibuta, Y.; Suzuki, T. A Molecular Dynamics Study of Thermodynamic and Kinetic Properties of Solid−Liquid Interface for Bcc Iron. *ISIJ Int.* **2010**, *50*, 1158−1164.
(66) Liu, J.; Davidchack, R. L.; Dong, H. B. Molecular Dynamics Calculation of Solid-Liquid Interfacial Free Energy and its Anisotropy during Iron Solidification. *Comput. Mater. Sci.* **2013**, *74*, 92−100.
(67) Pan, H.; Grigoropoulos, C. Crystallization in Nano-Confinement Seeded by a Nanocrystal − A Molecular Dynamics Study. *J. Appl. Phys.* **2014**, *115*, 104307.
(68) Espinosa, J. R.; Vega, C.; Valeriani, C.; Sanz, E. The Crystal-Fluid Interfacial Free Energy and Nucleation Rate of NaCl from Different Simulation Methods. *J. Chem. Phys.* **2015**, *142*, 194709.
(69) Zimmermann, N. E. R.; Vorselaars, B.; Quigley, D.; Peters, B. Nucleation of NaCl from Aqueous Solution: Critical Sizes, Ion-Attachment Kinetics, and Rates. *J. Am. Chem. Soc.* **2015**, *137*, 13352−13361.
(70) Zimmermann, N. E. R.; Vorselaars, B.; Espinosa, J. R.; Quigley, D.; Smith, W. R.; Sanz, E.; Vega, C.; Peters, B. NaCl Nucleation from Brine in Seeded Simulations: Sources of Uncertainty in Rate Estimates. *J. Chem. Phys.* **2018**, *148*, 222838.
(71) Lifanov, Y.; Vorselaars, B.; Quigley, D. Nucleation Barrier Reconstruction via the Seeding Method in a Lattice Model with Competing Nucleation Pathways. *J. Chem. Phys.* **2016**, *145*, 211912.
(72) Mizuguchi, T.; Higeta, Y.; Odagaki, T. Critical Nucleus Size for Crystallization of Supercooled Liquids in Two Dimensions. *Phys. Rev. E: Stat. Phys., Plasmas, Fluids, Relat. Interdiscip. Top.* **2017**, *95*, 042804.
(73) Wu, L.-K.; Li, Q.-L.; Li, M.; Xu, B.; Liu, W.; Zhao, P.; Bai, B.-Z. Calculation of Solid-Liquid Interfacial Free Energy and its Anisotropy in Undercooled System. *Rare Met.* **2018**, *37*, 543−553.
(74) Wedekind, J.; Strey, R.; Reguera, D. New Method to Analyze Simulations of Activated Processes. *J. Chem. Phys.* **2007**, *126*, 134103.
(75) Broughton, J. Q.; Gilmer, G. H. Molecular Dynamics Investigation of the Crystal-Fluid Interface. VI. Excess Surface Free Energies of Crystal-Liquid Systems. *J. Chem. Phys.* **1986**, *84*, 5759−5768.
(76) Plimpton, S. Fast Parallel Algorithms for Short-Range Molecular Dynamics. *J. Comput. Phys.* **1995**, *117*, 1−19.


DOI: 10.1021/acs.jpcc.8b10637
*J. Phys. Chem. C* 2018, 122, 28884−28894

(77) Davidchack, R. L.; Laird, B. B. Direct Calculation of the Crystal-Melt Interfacial Free Energies for Continuous Potentials: Application to the Lennard-Jones System. *J. Chem. Phys.* **2003**, *118*, 7651−7657.
(78) Morris, J. R.; Song, X. The Anisotropic Free Energy of the Lennard-Jones Crystal-Melt Interface. *J. Chem. Phys.* **2003**, *119*, 3920−3925.
(79) Asano, Y.; Fuchizaki, K. Phase Diagram of the Modified Lennard-Jones System. *J. Chem. Phys.* **2012**, *137*, 174502.
(80) Asano, Y.; Fuchizaki, K. Precise Determination of the Melting Point of a Modified Lennard-Jones System. *J. Phys. Soc. Jpn.* **2009**, *78*, 055002.
(81) Fuchizaki, K.; Asano, Y. Predicting the Thermodynamic Properties of the Modified Lennard-Jones Fluid from the Lennard-Jones equation of State. *J. Phys. Soc. Jpn.* **2013**, *82*, 124001.
(82) Asano, Y.; Fuchizaki, K. Modified Benedict-Webb-Rubin equation of State for the Modified Lennard-Jones Fluid. *J. Phys. Soc. Jpn.* **2014**, *83*, 034601.
(83) Asano, Y.; Fuchizaki, K. Determination of the Melting Curve of the Modified Lennard-Jones System Using the Nonequilibrium Relaxation Method. *J. Phys. Soc. Jpn.* **2017**, *86*, 025001.
(84) Protsenko, S. P.; Baidakov, V. G.; Tipeev, A. O. Melting Line, Spinodal and the Endpoint of the Melting Line in the System with a Modified Lennard-Jones Potential. *Thermophys. Aeromech.* **2013**, *20*, 93−104.
(85) Ushcats, M. V. Modified Lennard-Jones Model: Virial Coefficients to the 7th Order. *J. Chem. Phys.* **2014**, *140*, 234309.
(86) Laird, B. B.; Davidchack, R. L.; Yang, Y.; Asta, M. Determination of the Solid-Liquid Interfacial Free Energy along a Coexistence Line by Gibbs-Cahn Integration. *J. Chem. Phys.* **2009**, *131*, 114110.
(87) Espinosa, J. R.; Vega, C.; Sanz, E. The Mold Integration Method for the Calculation of the Crystal-Fluid Interfacial Free Energy from Simulations. *J. Chem. Phys.* **2014**, *141*, 134709.
(88) Angioletti-Uberti, S.; Ceriotti, M.; Lee, P. D.; Finnis, M. W. Solid-Liquid Interface Free Energy through Metadynamics Simulations. *Phys. Rev. B: Condens. Matter Mater. Phys.* **2010**, *81*, 125416.
(89) Benjamin, R.; Horbach, J. Crystal-Liquid Interfacial Free Energy via Thermodynamic Integration. *J. Chem. Phys.* **2014**, *141*, 044715.
(90) Rein ten Wolde, P.; Ruiz-Montero, M. J.; Frenkel, D. Numerical Calculation of the Rate of Crystal Nucleation in a Lennard-Jones System at Moderate Undercooling. *J. Chem. Phys.* **1996**, *104*, 9932−9947.
(91) Steinhardt, P. J.; Nelson, D. R.; Ronchetti, M. Bond-Orientational Order in Liquids and Glasses. *Phys. Rev. B: Condens. Matter Mater. Phys.* **1983**, *28*, 784−805.
(92) Malek, S. M. A.; Morrow, G. P.; Saika-Voivod, I. Crystallization of Lennard-Jones Nanodroplets: From Near Melting to Deeply Supercooled. *J. Chem. Phys.* **2015**, *142*, 124506.
(93) Maltsev, I.; Mirzoev, A.; Danilov, D.; Nestler, B. Atomistic and Mesoscale Simulations of Free Solidification in Comparison. *Modell. Simul. Mater. Sci. Eng.* **2009**, *17*, 055006.
(94) Schmelzer, J. W. P.; Boltachev, G. Sh.; Baidakov, V. G. Classical and Generalized Gibbs' Approaches and the Work of Critical Cluster Formation in Nucleation Theory. *J. Chem. Phys.* **2006**, *124*, 194503.
(95) Schmelzer, J. W. P.; Abyzov, A. S. Crystallization of Glass-Forming Melts: New Answers to Old Questions. *J. Non-Cryst. Solids* **2018**, *501*, 11−20.
(96) Moroni, D.; ten Wolde, P. R.; Bolhuis, P. G. Interplay Between Structure and Size in a Critical Crystal Nucleus. *Phys. Rev. Lett.* **2005**, *94*, 235703.
(97) Schmelzer, J. W. P.; Abyzov, A. S. Crystallization of Glass-Forming Liquids: Thermodynamic Driving Force. *J. Non-Cryst. Solids* **2016**, *449*, 41−49.
(98) Schmelzer, J. W. P.; Abyzov, A. S. Crystallization of Glass-Forming Liquids: Specific Surface Energy. *J. Chem. Phys.* **2016**, *145*, 064512.
(99) Tipeev, A. O. Crystallization of a Supercooled Liquid in Molecular Dynamics Models. Ph.D. thesis, Institute of Thermal Physics UB RAS, Ural Federal University, 2016.
(100) Baidakov, V. G.; Protsenko, S. P.; Tipeev, A. O. Temperature Dependence of the Crystal-Liquid Interfacial Free Energy and the Endpoint of the Melting Line. *J. Chem. Phys.* **2013**, *139*, 224703.
(101) Trudu, F. Computer Simulation Study of Homogeneous Nucleation in a Lennard-Jones Fluid, Ph.D. thesis, Swiss Federal Institute of Technology, 2006.
(102) Auer, S.; Frenkel, D. Numerical Prediction of Absolute Crystallization Rates in Hard-Sphere Colloids. *J. Chem. Phys.* **2004**, *120*, 3015−3029.
(103) Somorjai, G. A.; Li, Y. *Introduction to Surface Chemistry and Catalysis*, 2nd ed.; Wiley, 2010.
(104) Song, H.; Sun, Y.; Zhang, F.; Wang, C. Z.; Ho, K. M.; Mendelev, M. I. Nucleation of Stoichiometric Compounds from Liquid: Role of the Kinetic Factor. *Phys. Rev. Materials* **2018**, *2*, 023401.
(105) Haji-Akbari, A. Forward-Flux Sampling with Jumpy Order Parameters. *J. Chem. Phys.* **2018**, *149*, 072303.
(106) Fokin, V. M.; Zanotto, E. D.; Schmelzer, J. W. P. Homogeneous Nucleation versus Glass Transition Temperature of Silicate Glasses. *J. Non-Cryst. Solids* **2003**, *321*, 52−65.
(107) Schmelzer, J. W. P.; Abyzov, A. S.; Fokin, V. M.; Schick, C.; Zanotto, E. D. Crystallization in Glass-Forming Liquids: Effects of Fragility and Glass Transition Temperature. *J. Non-Cryst. Solids* **2015**, *428*, 68−74.
(108) Baidakov, V. G. Crystallization of Undercooled Liquids: Results of Molecular Dynamics Simulations. In *Glass: Selected Properties and Crystallization*; Schmelzer, J. W. P., Ed.; De Gruyter: Berlin, 2014; pp 481−520.


DOI: 10.1021/acs.jpcc.8b10637
*J. Phys. Chem. C* 2018, 122, 28884−28894